Scalable synthesis of activated carbon with superparamagnetic properties†

Manfred Schwickardi, Stefan Olejnik, Elena-Lorena Salabas, Wolfgang Schmidt and Ferdi Schüth*

Received (in Cambridge, UK) 9th June 2006, Accepted 19th July 2006
First published as an Advance Article on the web 8th August 2006
DOI: 10.1039/b608231a

Magnetic activated carbons were obtained by *in situ* formation of coated superparamagnetic iron nanoparticles in the pores of carbons initially impregnated with ferric salt solution.

Activated carbons are widely used as adsorbents, catalyst supports and as bio-compatible materials. For catalysis, purification of liquids or medical applications, the separation of the carbons from the fluid is crucial. The use of magnetic carbons allows separation by simply applying a magnetic field. For this reason, several groups started investigating the magnetic properties of carbon materials. There are two pathways to obtain magnetic carbon. The first is based on the ferromagnetic properties of pure carbon materials.[1] The magnetization of such carbon materials is rather low, and therefore the alternative, composites of carbon materials with magnetic particles, seems to be more promising for technical applications. Deposition of magnetic oxide particles on carbon nanotubes has been reported[2] as well as formation of magnetic oxides in the pores of activated carbons.[3] However, the magnetic particles decorating the carbon materials are easily dissolved and/or washed out by acidic solutions. Protective coatings of the magnetic particles are a feasible method to overcome this drawback. By deposition of preformed cobalt nanoparticles on a mesoporous carbon support followed by carbon coating of the cobalt particles, it was possible to obtain a chemically stable and magnetically separable carbon material. Additional deposition of palladium on the magnetic carbon resulted in a magnetically separable hydrogenation catalyst.[4] Also the coating of magnetic cobalt nanoparticles by carbon of different origin is a possibility for obtaining such materials, which have, however, a rather high metal content.[5] The pathways based on cobalt nanoparticles are rather complex, since the nanoparticles need to be synthesized first by liquid phase reactions under a protective atmosphere before they can be further processed. Magnetic monodispersed carbon nanoparticles on a relatively large scale or magnetic carbon nanotubes have been synthesized by pyrolysis of polypyrrole which contains iron oxide.[6] However, the surface areas of these materials were relatively small *i.e.* 360 m^2 g^{-1}, since the aim was the production of carbon nanoparticles, not that of a magnetic activated carbon. Here, we present an easy and scalable method for the preparation of bulk quantities of superparamagnetic activated carbon with well-protected iron particles as the magnetic component and high specific surface area.

The method consists of a series of simple preparation steps starting from an activated carbon which is impregnated with aqueous iron(III) solution, followed by drying and calcination under inert atmosphere. During the calcination iron particles are formed in the pores of the carbon, which are then coated with a carbon layer formed by CVD using benzene as carbon precursor.

In a typical preparation, 20 g of a microporous activated carbon (Kugelkohle, Blücher GmbH) which had been exposed to a second activation step in N_2–H_2O at 900 °C and having an apparent specific surface area of 2099 m^2 g^{-1} was impregnated under stirring with 16 mL of 2.33 M $Fe(NO_3)_3$ solution. The solution was completely absorbed by the carbon upon continued intense stirring for 5 min. After drying at 90 °C, the impregnated carbon was transferred into a rotary oven (quartz glass tube, see ESI†) and heated (4.5 °C min^{-1}) to a temperature of 700 °C under argon. After reaching this temperature, rotation of the tube was started and benzene vapor was flowed through the tube. The activated carbon material was agitated for 30 min in the rotation tube in the argon–benzene flow (1.87 mmol min^{-1}). After cooling to room temperature, 22.13 g of product were obtained. The apparent specific surface area of the carbon material was reduced to 1642 m^2 g^{-1} after this treatment (see ESI). Upon calcination under argon atmosphere, elemental iron particles are formed in the pores of the activated carbon as evidenced by the XRD patterns shown in Fig. 1.

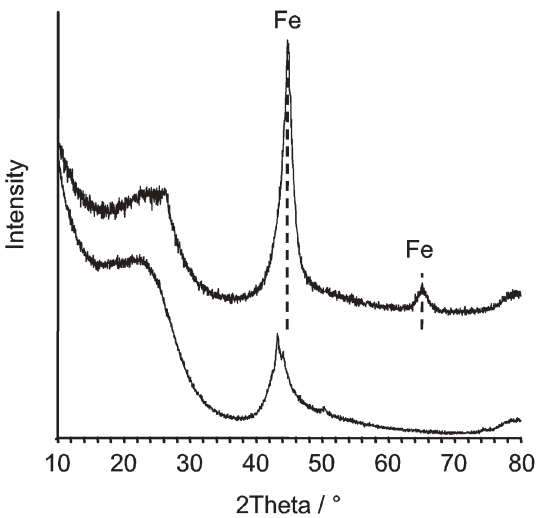

Fig. 1 XRD patterns of parent activated carbon (bottom) and the composite containing Fe particles in activated carbon (top) obtained in the lab rotary oven. The dashed line indicates the position of Fe reflections.

Max-Planck-Institut für Kohlenforschung, Kaiser-Wilhelm-Platz 1, D-45470, Mülheim an der Ruhr, Germany.
E-mail: schueth@kofo.mpg.de; Fax: +49 208 306 2995;
Tel: +49 208 306 2373

† Electronic supplementary information (ESI) available: Photographs of the laboratory rotary oven and the pilot scale rotary kiln, nitrogen sorption isotherms of the parent activated carbon and the magnetic carbon. See DOI: 10.1039/b608231a

The iron particles in the carbon material are very resistant against leaching and dissolution. Upon treatment with 2 M HNO_3 solution only 3% of the iron present in a typical material obtained in the lab rotary oven was dissolved. The iron particles are obviously well-protected by the carbon shells. A material which had not been treated with benzene vapor (no protective carbon shell) lost more than 90% of the iron under the same conditions.

The majority of the iron particles have sizes of less than 10 nm as evidenced by the broad XRD reflections and the TEM image shown in Fig. 2 (top). Occasionally also larger particles are observed.

Visualization of the carbon shells of iron particles inside the activated carbon is difficult because of the more or less identical absorption contrast of the shell and the carbon host but occasionally particles are found also on the external surface of the activated carbon as shown by the high resolution TEM image (Fig. 2, bottom). The lattice planes of the iron particles and the graphene sheets in the surrounding carbon shells are clearly discernible.

The small size of the iron particles results in superparamagnetic properties. In order to identify the transition temperature (blocking temperature) from the ferromagnetic state to the superparamagnetic state, the zero-field cooled (ZFC) magnetization as a function of temperature was measured using a superconducting quantum interference device magnetometer (SQUID). For the ZFC experiment, the sample was cooled in zero field from room temperature to 2 K. This implies that by decreasing the temperature the particle moments are blocked progressively along their anisotropy directions. After reaching T = 2 K the magnetization is recorded on warming and in a weak external field of 20 Oe. The observed temperature-dependent magnetization is shown in Fig. 3.

The ZFC curve shows a peak at about 50 K which corresponds to the blocking temperature of the assemblies of the single-domain Fe nanoparticles. In principle, particle sizes can be obtained from the blocking temperature, if the particles are magnetically isolated and monodisperse. However, this is not the case for our samples due to the relatively high concentration of iron particles and the size distribution, and therefore, no correlation of blocking temperature and the particle sizes determined by TEM was attempted.

The hysteresis loop measured at 5 K (Fig. 4) shows the ferromagnetic behavior of the material with a saturation magnetization of about 18 emu g^{-1} and a coercivity of about 220 Oe. Remanence magnetization of about 4.3 emu g^{-1} has been measured. The field-cooled hysteresis loop (not shown) was not shifted along the field axis indicating the absence of an exchange bias effect. The lack of this exchange coupling implies that the Fe nanoparticles are not surrounded by an oxide layer or that this layer is very thin (less than 2 nm).

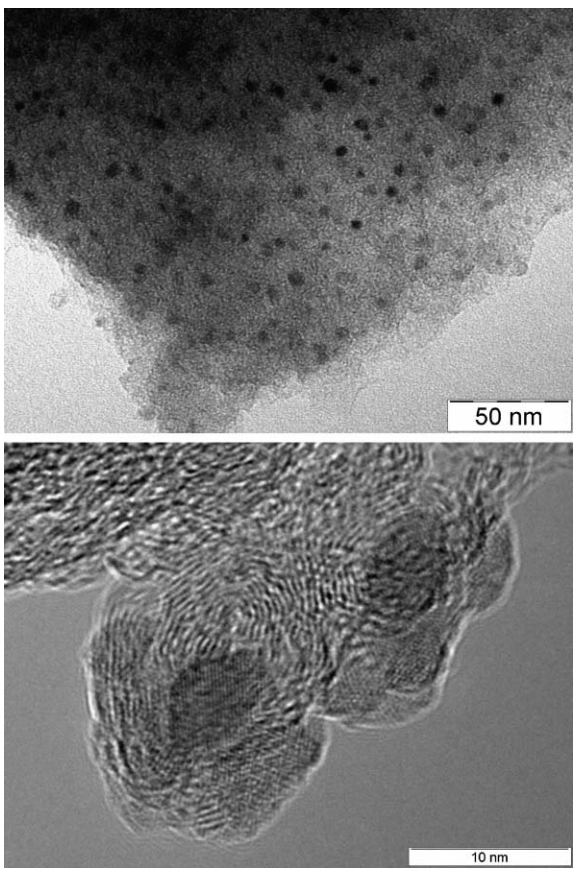

Fig. 2 TEM image of iron nanoparticles in the activated carbon matrix (top, scale bar 50 nm) and high resolution TEM image of iron particles with carbon shell (bottom, scale bar 10 nm).

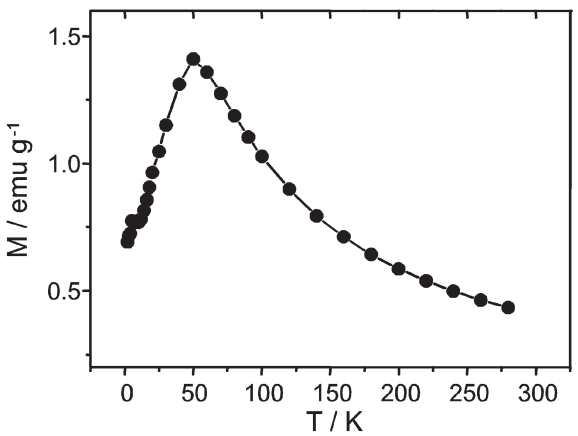

Fig. 3 Zero field cooled (ZFC) temperature dependent magnetization for Fe nanoparticles embedded in an activated carbon matrix measured at 20 Oe.

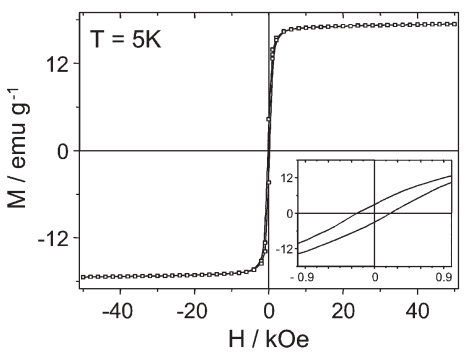

Fig. 4 Hysteresis loop at 5 K for Fe nanoparticles embedded in the activated carbon matrix. Inset shows the low field region of the hysteresis.

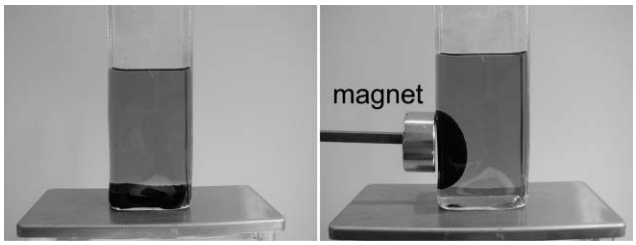

Fig. 5 Interaction of the magnetic carbon with a permanent magnet.

It should be noted that the iron–carbon composites also contain a small fraction of iron carbide as evidenced by XPS spectroscopy. This minor by-phase is probably formed on the surface of the iron particles during the calcination under protective atmosphere.

Fig. 5 shows the magnetic carbon sedimented in a solution (left) and attracted by a permanent magnet. After removing the permanent magnet, the carbon is easily redispersed in the solution because of the superparamagnetic properties of the iron particles. Their size in the range of a few nanometres prevents ferromagnetism because the size of the magnetic domains (<10 nm) falls below its critical value. At this size, the thermal energy at room temperature is sufficient to change the direction of magnetization of the entire crystallite at room temperature. In presence of a field, the magnetic momentum of the complete crystallite is aligned with the external field. After removal of the external magnetic field, the alignment of the magnetic momentum is lost, allowing redispersion of the particles. It should be noted that a small residual ferromagnetism at room temperature was observed which can be attributed to the small fraction of larger iron particles in the material. This, however, did not negatively affect the redispersibility of the materials.

The preparation of magnetic carbon as described above thus results in a material with excellent magnetic properties for various applications. The particles only aggregate in a magnetic field and redispersion occurs if the external magnetic field is switched off. In contrast to materials from other reports where the magnetic properties are due to metal oxide particles, here metallic iron nanoparticles are causing the magnetism. Also in contrast to most reports, a protective carbon shell prevents dissolution and/or leaching of the metal nanoparticles.

In order to prove the scalability of the preparation method, magnetic carbons were also synthesized on a larger scale in a pilot plant-size rotary kiln (see ESI†). For this preparation, 125 g of activated carbon (P-43 171, Adsor-Tech, 0.598 $cm^3\ g^{-1}$, 1207 $m^2\ g^{-1}$) was impregnated with 59.8 mL of 2 M $Fe(NO_3)_3$ solution and fed into the continuously operated rotary kiln. The impregnated 0.3–0.5 mm activated carbon beads are successively transferred through a drying zone, a decomposition zone, a calcination zone and a cooling zone. In order to prevent working with larger amounts of benzene, a nitrogen–toluene stream (N_2 flow 50 L h^{-1}) was passed at 700 °C in concurrent flow over the carbon material in the kiln. In this way, a magnetic carbon containing about 5 wt% of iron was obtained. The toluene acts in the same way as benzene. Using this pilot scale kiln, a productivity of about 25 g h^{-1} of magnetic carbon could be achieved. However, if working with higher loading as in the experiment described, the fraction of ferromagnetic domains increases.

The materials obtained *via* the pathway described in this manuscript are essentially superparamagnetic, have high surface areas and high porosities, they are bio-compatible, and stable under alkaline as well as under acidic conditions. Last but not least, upscaling of the preparation process is easily possible. This makes these magnetic carbons very promising candidates for larger scale applications in catalysis (*e.g.* magnetically separable catalyst supports) and/or separation technology (*e.g.* magnetically separable adsorber).

Notes and references

1 T. L. Makarova, *Semiconductors*, 2004, **38**, 615–638; H. Pardo, R. Faccio, F. M. Araújo-Moreira, O. F. de Lima and A. W. Mombrú, *Carbon*, 2006, **44**, 565–569; P. Esquinazi, K. H. Han, R. Höhne, D. Spemann, A. Setzer and T. Butz, *Phase Transitions*, 2005, **78**, 155–168.
2 L. C. A. Oliveira, R. V. R. A. Rios, J. D. Fabris, V. Garg, K. Sapag and R. M. Lago, *Carbon*, 2002, **40**, 2177–2183; Z. Sun, Z. Liu, Y. Wang, B. Han, J. Du and J. Zhang, *J. Mater. Chem.*, 2005, **15**, 4497–4501; C. Gao, W. Li, H. Morimoto, Y. Nagaoka and T. Maekawa, *J. Phys. Chem. B*, 2006, **110**, 7213–7220.
3 A. B. Fuertes and P. Tartaj, *Chem. Mater.*, 2006, **18**, 1675–1679.
4 A.-H. Lu, W. Schmidt, N. Matoussevitch, H. Bönnemann, B. Spliethoff, B. Tesche, E. Bill, W. Kiefer and F. Schüth, *Angew. Chem., Int. Ed.*, 2004, **43**, 4303–4306.
5 A.-H. Lu, W.-C. Li, N. Matoussevitch, B. Spliethoff, H. Boennemann and F. Schüth, *Chem. Commun.*, 2005, 98–99.
6 J. Jang and H. Yoon, *Small*, 2005, **1**, 1195–1199; J. Jang and H. Yoon, *Adv. Mater.*, 2003, **15**, 2088–2091.